Research on wind turbine blade damage based on pre-stressed FBG strain sensors*

CAI Yujie[1,2,3], YANG Zhiquan[2], ZHANG Bihua[3], and WEI Yufeng[3]**

1. Faculty of Land Resources Engineering, Kunming University of Science and Technology, Kunming 650093, China

2. Faculty of Public Safety and Emergency Management, Kunming University of Science and Technology, Kunming 650093, China

3. Beijing FBGTECH Optic Electric Technology Co., Ltd., Beijing 100043, China

(Received 16 May 2023; Revised 9 August 2023)

One of the essential parts of a wind power generator that captures wind energy is the wind turbine blade. The safety of the blades rapidly declines as a wind turbine's operating period grows. For real-time monitoring, a chip-type pre-stressed fiber Bragg grating (FBG) strain sensor was fabricated. The sensor's structure was improved using simulation analysis along with optimization. It was discovered through calibration trials that the pre-stressing method expanded the sensor's range of measurement, guaranteed overall linearity, and prevented the potential hysteresis phenomena during compression. The sensor's final sensitivity was calculated to be 1.970 pm/με, and its linear fitting coefficient was 0.999. Finally, the sensor was used to monitor the wind turbine blades and the strain change curve of the root of a normally functioning blade is found to be a sine curve, which provides a certain reference value for judging whether the blade is damaged in the future.

Document code: A **Article ID:** 1673-1905(2024)02-0083-6

DOI https://doi.org/10.1007/s11801-024-3093-6

Wind energy has emerged as a prominent renewable energy source and has gained considerable traction as a primary contributor to electrical power generation[1]. The global capacity of wind turbine installations is consistently expanding, reflecting the growing reliance on wind power[2]. However, as wind turbine blades accumulate service time, they are subjected to fatigue and damage, highlighting the need for real-time monitoring to assess their structural health.

Currently, the monitoring of blade damage in wind turbines primarily relies on methods such as strain monitoring, vibration monitoring, and ultrasonic detection techniques[3]. Among these, strain monitoring is widely used globally and involves attaching or embedding sensors on/in the blades to measure strain. Traditional strain measurements rely on resistance strain gauges, which are prone to electromagnetic interference and long-term monitoring failures, leading to inaccurate results. In contrast, fiber Bragg gratings (FBGs) offer advantages such as simple structure, immunity to electromagnetic interference, stability, and networking capabilities[4]. FBG sensors are particularly suitable for long-term, real-time monitoring of wind turbine blades with extended service periods. They provide continuous and reliable strain measurements for detecting structural changes, facilitating proactive maintenance and timely repairs to ensure optimal performance and safety.

In practical engineering applications, the susceptibility of FBGs to shear forces, external damage, low sensitivity, and limited measurement range necessitates their encapsulation. Currently, both domestic and international approaches to FBG encapsulation can be classified into three categories: substrate-based packaging[5], tube-based packaging[6], and embedded packaging[7]. Among these methods, substrate-based packaging stands out due to its simplicity in sensor structure, ease of fabrication, and the ability to monitor completed structures without causing secondary damage. Significant research has been conducted on substrate-based packaging of FBG sensors. For example, LU et al[8] designed pre-stretched substrate-based FBG sensors with a strain sensitivity of 0.95 pm/με and a linearity of 0.996. These sensors were successfully applied to aircraft wing I-beams, providing strain values consistent with simulation results. LI et al[9] employed simulation analysis to design an innovative enhanced sensitivity structure for strain gauges, achieving a strain sensitivity 3.4 times higher than traditional "I"-shaped strain gauges. PENG et al[10] focused on lithium

* This work has been supported by the National Natural Science Foundation of China (No.41861134008), the Muhammad Asif Khan Academician Workstation of Yunnan Province (No.202105AF150076), the Key R&D Program of Yunnan Province (No.202003AC100002), the General Program of Basic Research Plan of Yunnan Province (No.202001AT070043), the Science and Technology Talents and Platform Program of Yunnan Province (No.202305AD160064), and the Basic Research Project of Yunnan Province (No.202201AT070283).

** E-mail: yzq1983816@kust.edu.cn

batteries and developed a micro-strain measurement sensor utilizing lever principles, flexible hinges, and serpentine springs. This novel design significantly increased the strain sensitivity to 11.49 pm/με, while maintaining a high linearity of 0.999.

The study focuses on the damage monitoring of wind turbine blades by the substrate-based pre-stressed FBG. The dimensions of the substrate and incorporate pre-stretching of each bare fiber grating are optimized, and the sensor underwent calibration in a controlled laboratory environment to assess its performance indicators. The calibrated sensor was then deployed in an engineering environment to monitor the strain at the root of wind turbine blades. To evaluate the structural integrity of the wind turbine blades, the real-time stress values were calculated by combining the stress-strain relationship. These calculated stress values were then compared with the allowable stress, which provided a theoretical foundation for determining whether the blade is damaged in subsequent assessments. By employing substrate-based pre-stressed FBG strain sensors, conducting simulation analysis, and applying data processing techniques, this study aimed to enhance the understanding and monitoring of strain in wind turbine blades, ultimately contributing to the assessment of their structural health and integrity.

The FBG sensor consists of a quartz fiber material, comprising a core, cladding, and coating, as illustrated in Fig.1. The central element of the FBG sensor is the Bragg grating region. As the light signal emitted by the light source enters the FBG region, the light of a specific wavelength, known as the center wavelength, meets the reflection condition, while light of other wavelengths is transmitted, leading to the formation of a transmission spectrum.

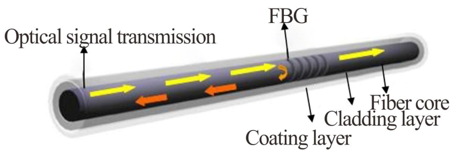

Fig.1 Principle of the FBG sensing

By applying the theory of coupled wave fields, it can be deduced that the center wavelength of the reflected light from the FBG depends on the grating period and the effective refractive index of the fiber core. The expression for the center wavelength is given as[11]

$$\lambda_B = 2n_{eff}\Lambda, \tag{1}$$

where λ_B represents the center wavelength of the FBG, n_{eff} denotes the effective refractive index of the fiber core, and Λ represents the grating period. Assuming the fiber undergoes uniform axial deformation, the relationship between the center wavelength drift, strain, and temperature in the FBG can be expressed as

$$\frac{\Delta\lambda_B}{\lambda_B} = (1 - P_e)\varepsilon+(\xi+\alpha)\Delta T. \tag{2}$$

In the above equation, $\Delta\lambda_B$ signifies the wavelength change, P_e refers to the effective piezo-optic coefficient of the fiber, ξ represents the thermal-optic coefficient of the fiber, and α represents the coefficient of thermal expansion of the fiber.

This study introduces a novel substrate design for the FBG strain sensor, as depicted in Fig.2, to protect the bare optical fiber. The substrate exhibits overall dimensions of 83.5 mm in length, 20 mm in width, and 1.5 mm in thickness, utilizing 304 stainless steel renowned for its exceptional weldability and extensive applicability. The design concept entails embedding the grating within the intermediate groove of the substrate, while a spring-like structure with reduced stiffness is incorporated to enhance sensitivity to minute strains and facilitate transmission to the optical fiber. Moreover, compared to the conventional "I-beam" shaped substrate, the square-shaped tabs on both sides have been enlarged, providing an increased adhesive surface area for enhanced structural integrity during assembly. Additionally, the cross-shaped structures on the sides offer alternative installation options, enabling connection to the target object through welding, if feasible for the specific structure being tested.

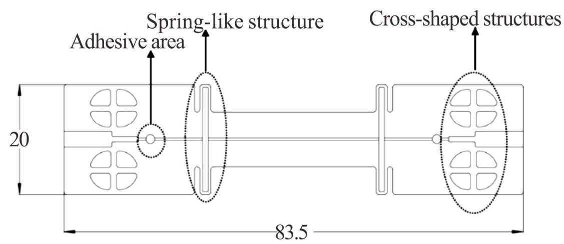

Fig.2 Structure diagram of the substrate-based FBG strain sensor

During the substrate design phase, Creo 7.0 was utilized for three-dimensional modeling of the sensor. Finite element analysis of the substrate was performed using ANSYS WORKBENCH 2022 R1 to determine the dimensions of the spring-like structure. The simulation process employed sweeping for mesh generation of the substrate. For boundary conditions, a strain of 1 000 με was assumed, and the effective length of the sensor was set to 52 mm. Consequently, displacements of 0.026 mm were applied at both ends along the x-axis. The resulting strain cloud map of the substrate is illustrated in Fig.3.

Based on the strain cloud map, it can be observed that no strain mutation occurred in the region where the grating was positioned during the stretching of the substrate. Hence, it can be inferred that the optical fiber grating experienced uniform strain in the force-bearing region, while stress concentration was observed in the spring-like structure, thereby achieving the desired outcome. By means of simulated analysis, the overall width of the spring-like structure is 2 mm, with a central hollow width of 1 mm, as depicted in Fig.4. This outcome not only takes into account the prompt feedback capability of the spring-like structure for micro-strains, but also considers the processing difficulties during manufacturing.

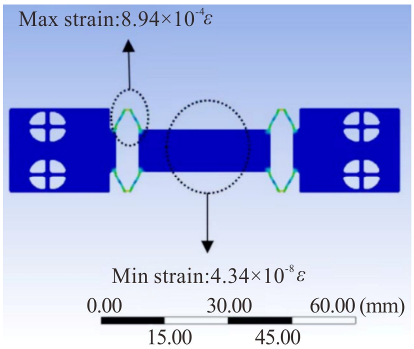

Fig.3 Cloud map of substrate strain

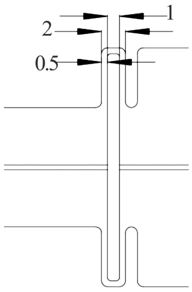

Fig.4 Dimensional diagram of the spring-like structure

Fig.5(a) illustrates a cross-sectional diagram of the substrate-based FBG strain sensor along with the tested specimen. In the analytical process, it is assumed that all materials involved are isotropic and exhibit a strong bond between layers. Specifically, the tested specimen is subject to direct external axial forces, while all other strains are transmitted through shear strain. Fig.5(b) illustrates the axial force analysis between layers of the sensor, where $2L$ represents the length of the adhesive layer. The subscripts f, p, v, b, z and o denote the fiber grating, protective layer, fiber adhesive layer, encapsulation substrate layer, substrate adhesive layer, and tested substrate layer, respectively. $\tau(x, r)$, σ_x, ε, $\mathrm{d}\sigma$ and r represent the shear stress between different layers, axial stress, strain, axial stress for each layer as an element, and the variable along the radial length of the fiber, respectively.

Taking a differential element dx along the x-axis direction of the substrate-based FBG strain sensor, mechanical analysis is conducted on each layer. Ultimately, the average strain transmission formula is obtained as

$$\bar{\beta}(x) = 1 - \frac{\sinh(kL)}{kL\cos(kL)}, \tag{3}$$

where k is the strain lag coefficient[12]. Eq.(3) indicates that the main factors affecting the transmission coefficient are the thickness h of each layer and the length L of the adhesive. As a result, achieving uniform thickness across all layers of the sensor during the manufacturing process is impractical, and ensuring a secure bond between the tested specimen and the sensor during construction presents challenges. Hence, it becomes crucial to consider the strain transmission relationship of the strain sensor.

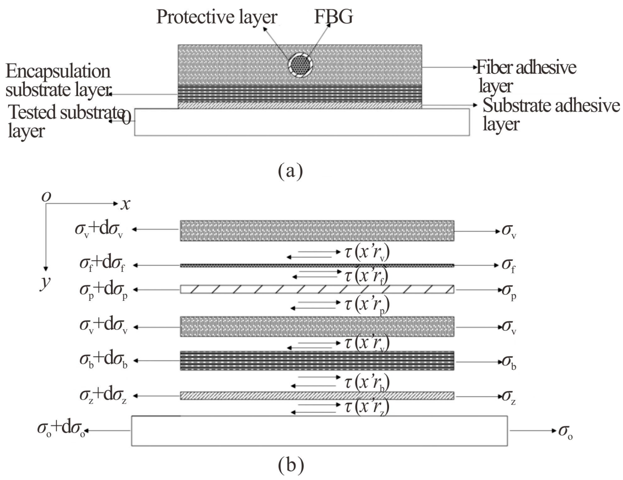

Fig.5 Schematic diagram of the layered structure of the substrate-type FBG strain sensor and axial force analysis: (a) Cross-sectional side view; (b) Axial force diagram

Based on the aforementioned structural optimization, the fabrication process of the substrate-based FBG strain sensor is conducted. To prevent undesired effects such as chirping or multimode phenomena in the reflected spectrum of the FBG sensor, pre-stretching of the bare fiber is implemented during the preparation stage. In consideration of the strain transfer between the fiber grating and the substrate, a thermosetting epoxy resin adhesive called 353ND is chosen for bonding the bare fiber to the substrate[13]. A heating and packaging platform, as shown in Fig.6, is designed to heat-cure the epoxy resin adhesive 353ND during the packaging process, and the finished sensor is shown in Fig.7.

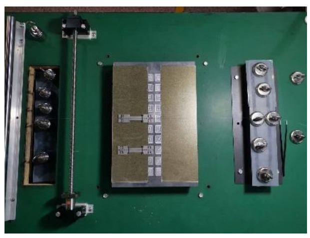

Fig.6 Sensor encapsulation diagram

Subsequent to the encapsulation process, the sensor's center wavelength-strain sensitivity and linearity can be altered, necessitating calibration after the fabrication of the sensor. To establish alignment between the strain values obtained from the strain gauge and the sensor, a calibration experiment was conducted using an equally robust cantilever beam. In this experiment, the strain gauge recorded the strain values from the gauge, while the center wavelength of the sensor was collected and demodulated using a fiber grating demodulator. Specifically, the FAS-C high-speed fiber grating intelligent demodulator from Beijing FBGTECH Optic Electric Technology Co., Ltd. was employed, with a remarkable resolution of 0.1 pm. The demodulation principle is depicted in Fig.8, providing a visual representation of the process.

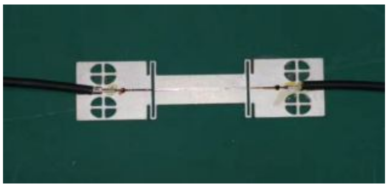

Fig.7 The finished FBG-based sensor

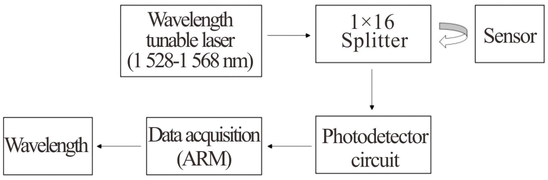

Fig.8 Principle of the demodulator

After establishing the calibration system, the cantilever beam was incrementally loaded, with a one-minute interval between each load to allow for the stabilization of the sensor's center wavelength before the subsequent loading. The loading process was conducted stepwise until a strain of 1 000 με was reached, followed by a stepwise unloading process. The outcomes of a single loading and unloading test are depicted in Fig.9. As illustrated in Fig.9(a), the pre-stretched sensor demonstrates a favorable linearity between the center wavelength and strain throughout the loading and unloading process. In contrast, Fig.9(b) reveals that the non-pre-stretched sensor exhibits poor linearity within the range of a—b and c—d, while displaying good linearity within the range of b—e and e—c. This phenomenon can be attributed to the fact that the non-stretched fiber grating region remains in a relaxed state, with minimal changes in grating distance under slight strain, resulting in diminished linearity between the center wavelength and strain. However, when subjected to larger strains, the grating region experiences tension, leading to improved linearity between the center wavelength and strain. Consequently, the pre-stretching process is adopted to enhance the measurement range of the sensor and ensure consistent linearity throughout the entire measurement range.

The loading and unloading tests were repeated three times, and the final fitting of the changes in the center wavelength and strain of the sensor is shown in Fig.10, indicating that the sensor remains within the linear range during the loading and unloading tests. Therefore, the average value of the three tests was taken, resulting in a sensitivity of 1.970 pm/με and a linear fitting coefficient of 0.999 for the sensor.

The FBG sensor is susceptible to temperature effects, thus requiring temperature calibration of the encapsulated sensor. Placing the sensor inside a high-low temperature test chamber, the initial temperature was set at −40 °C, with the final value set at 80 °C. The temperature was incremented by 20 °C each time, and at each temperature point, it was maintained for 30 min. Data was recorded once the wavelength stabilized. The results are depicted in Fig.11.

From the illustration, it is apparent that within the temperature range from −40 °C to 80 °C, the central wavelength exhibits a linear variation with temperature. The coefficient of temperature sensitivity is calculated to be 14.921 pm/°C, indicating a strong linear correlation. Moreover, the sensor operates reliably within the temperature range from −40 °C to 80 °C, demonstrating its suitability for demanding environments characterized by high and low temperatures. The fabricated sensor is applied in a pilot project at a wind farm. The wind turbine model used in this pilot project is the GOLDWIND 1500 wind turbine, with a service life of approximately 15 years. Based on the pilot project, the following sensor installation scheme has been selected. For each blade, four FBG strain sensors and four FBG temperature sensors (for temperature compensation, Fig.12) are installed at a distance of 1.5 m from the blade root, and each sensor is bonded on the blade with specialized adhesive.

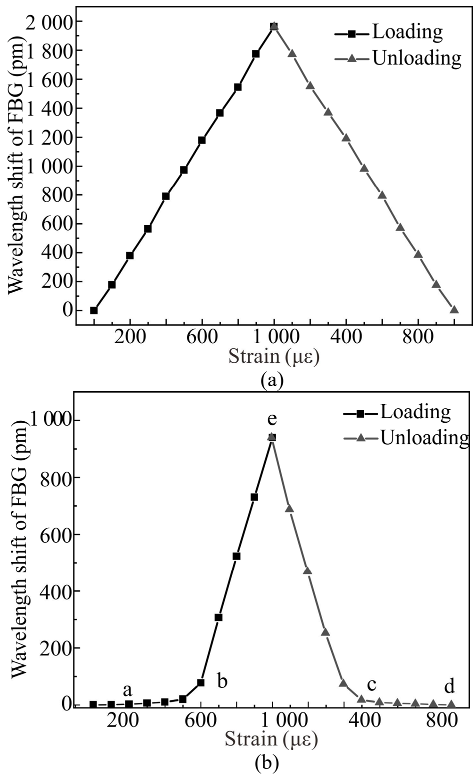

Fig.9 (a) Wavelength variation plot of pre-stretched optical fiber during loading and unloading; (b) Wavelength variation plot of unstretched optical fiber

Once all sensors are properly affixed, they are connected to the demodulator in the hub cabinet. A waiting period of 24 h is observed to ensure a complete bonding between the adhesive and the blade. This measure is taken to prevent sensor detachment during blade rotation, which could lead to inaccurate data or potential damage to the turbine.

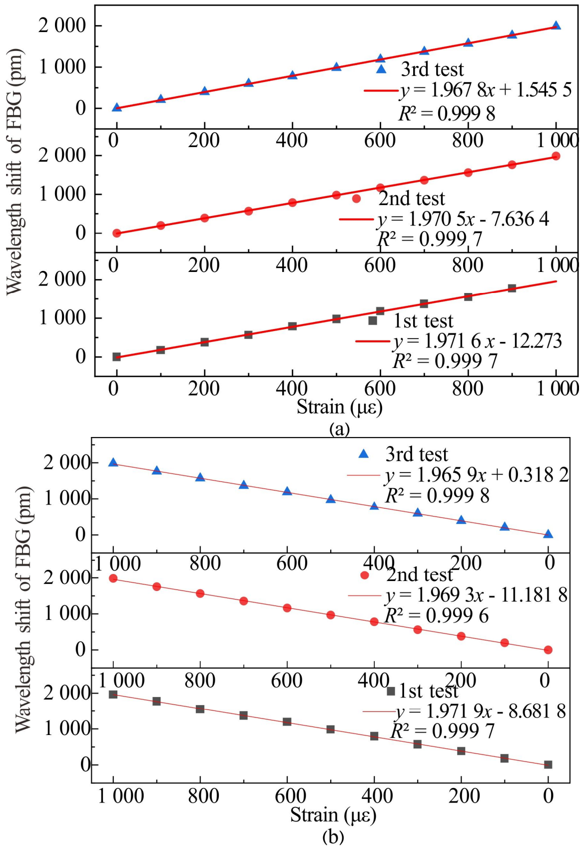

Fig.10 Three experiments and fitting results: (a) Loading test; (b) Unloading test

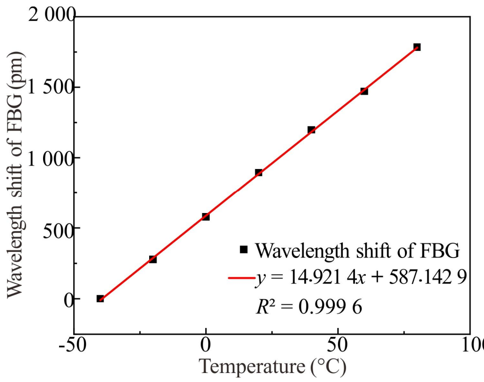

Fig.11 Temperature fitting results

The demodulator selected for this pilot project is the FAS-C demodulator, which was used during calibration. The sampling frequency is 10 Hz. Based on the data points collected at a rate of 10 points per second, a strain variation plot of the wind turbine blade root during normal operation was generated. Fig.13(a) depicts the strain variation of blade A within the time interval of 0 to 1.3×10^5 s. From 0 to 2.3×10^4 s, the wind turbine in a free state, and the wind speed was relatively low. During this period, the blades were not subjected to strong external forces, resulting in relatively small measured strain data. From 2.3×10^4 s to 5×10^4 s, the wind turbine was in a locked state, and the blades were in a relatively static state without significant external forces. Therefore, the strain remained relatively constant during this time interval. After 5×10^4 s, the wind turbine started operating normally, experiencing its own driving forces as well as external wind forces. This led to significant tensile and compressive strains within the monitoring interval, resulting in larger strain variations.

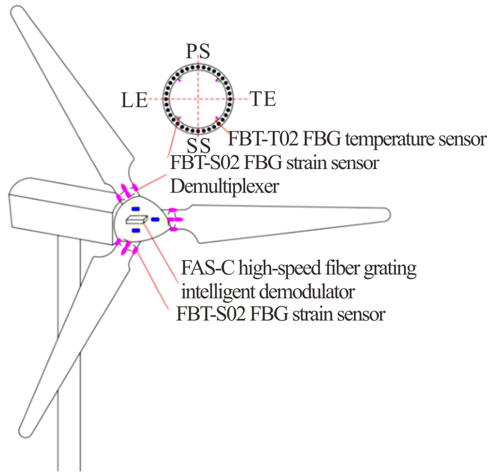

Fig.12 Sensor installation diagram

Fig.13(b) depicts the temporal fluctuations within a span of 100 s during the stable operation of the wind turbine. The PS side represents the windward side, primarily subjected to tensile loads, while the SS side represents the leeward side, primarily experiencing compressive loads. It can be observed from the figure that the data aligns with the stress state of the wind turbine blade structure. Additionally, it is evident that during normal operation, the strain curve follows a smooth sinusoidal pattern. According to the rotational speed displayed in the control room for the wind turbine blade, it was discovered that the period of the sinusoidal wave corresponds to the rotational speed of the wind turbine blade. The finding is consistent with the monitoring results of indoor simulated blade experiments conducted by Kerstin Schroeder[14].

In the elastic regime of a material, the relationship between stress and strain is linearly proportional. Through indoor testing, the elastic modulus of the wind turbine blade can be determined. When coupled with strain monitoring, the stress levels within the blade can be evaluated. By comparing the obtained stress levels with the allowable stress limit specified for the blade, it becomes possible to assess the presence of long-term damage. If the stress exceeds the allowable limit, it indicates the potential occurrence of structural degradation or other forms of damage over time. This approach enables the identification of critical stress conditions and facilitates proactive maintenance and intervention to ensure the structural integrity and performance of the wind turbine blade.

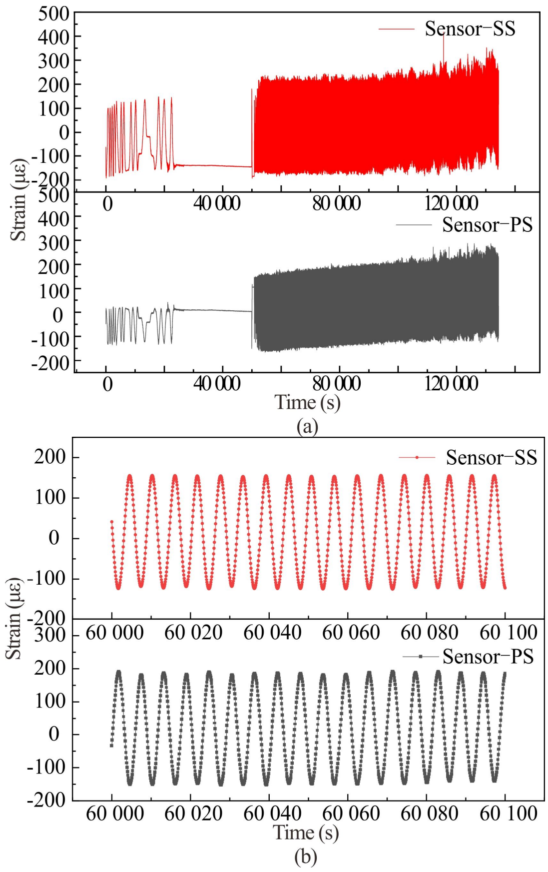

Fig.13 Monitoring results: (a) Overall results; (b) Partial results

This letter aims to address the limitations of conventional methods for monitoring wind turbine blade damage and proposes an innovative approach utilizing a substrate-based pre-stressed FBG strain sensor. The sensor's structure was optimized through simulation analysis, and pre-stressing was implemented to mitigate the potential occurrence of wavelength chirping during compression deformation measurements. Following calibration experiments conducted on an equally robust cantilever beam, it was observed that pre-stressing expanded the measurement range and enhanced overall linearity, resulting in a final sensitivity of 1.970 pm/με and a linear fitting coefficient of 0.999. Subsequently, the sensor was employed to monitor strain in wind turbine blades, revealing sinusoidal curves on both the PS and SS surfaces at the root of the blades under normal operating conditions. By considering the stress-strain relationship, it can be inferred that prolonged exposure to stresses surpassing the allowable limits may lead to fatigue damage in the blades. Consequently, the proposed sensor holds valuable reference value in assessing potential blade damage in the future.

Ethics declarations

Conflicts of interest

The authors declare no conflict of interest.

References

[1] Global Wind Energy Council. 2014 China wind power review and outlook[R]. GWEC, 2014.

[2] Global Wind Energy Council. Global wind report 2022[R]. GWEC, 2022.

[3] BEGANOVIC N, SÖFFKER D. Structural health management utilization for lifetime prognosis and advanced control strategy deployment of wind turbines: an overview and outlook concerning actual methods, tools, and obtained results[J]. Renewable and sustainable energy reviews, 2016, 64: 68-83.

[4] SUN X, WANG Q M, LI Z W, et al. Abnormal diagnosis of fiber Bragg grating strain gauges in health monitoring system[J]. Optics and precision engineering, 2021, 29(11): 2581-2589.

[5] TAN Y G, CHEN Y Y, LI R Y, et al. A substrate-type fiber Bragg grating strain sensor with enhanced sensitivity[J]. Chinese journal of sensors and actuators, 2018, 31(6): 664-669.

[6] REN L, LI H G, HU Z Q, et al. Development and application of FBG strain sensor with enhanced sensitivity in the model vibration experiment[J]. Journal of optoelectronics·laser, 2008, 19(11): 1437-1441. (in Chinese)

[7] MIELOSZYK M, MAJEWSKA K, OSTACHOWICZ W, et al. Application of embedded fiber Bragg grating sensors for structural health monitoring of complex composite structures for marine applications[J]. Marine structures, 2021, 76: 102903.1-102903.17.

[8] LU L D, YAN G, LIU F, et al. Joist load test based on pre-stretching substrate FBG sensor[J]. Piezoelectrics & acoustooptics, 2017, 39(4): 619-623.

[9] LI Z Y, ZHANG Z P, ZHANG X P, et al. Research on the sensitivity structure of the substrate fiber grating strain sensor[J]. Optical communication technology, 2018, 42(6): 21-24.

[10] PENG J, JIA S, JIN Y, et al. Design and investigation of a sensitivity-enhanced fiber Bragg grating sensor for micro-strain measurement[J]. Sensors and actuators A: physical, 2019, 285: 437-447.

[11] MATVEENKO V P, SHARDAKOV I N, VORONKOV A A, et al. Measurement of strains by optical fiber Bragg grating sensors embedded into polymer composite material[J]. Structural control & health monitoring, 2018, 25(3): 1-11.

[12] DU C C, KONG D R, XU C D, et al. Design of metallic packaged fiber Bragg grating sensor and its strain transfer experiment[J]. Journal of Hunan University (natural sciences), 2022, 50(4): 9-20.

[13] DING C, LIANG J C, YIN Y N, et al. Surface treatment technology for enhancing adhesion between rubber and metal[J]. China synthetic rubber industry, 2013, 36(5): 405-410.

[14] KERSTIN S, WOLFGANG E, JORG A, et al. A fiber Bragg grating sensor system monitors operational load in a wind turbine rotor blade[J]. Measurement science and technology, 2006, 17(5): 1167-1172.